Low-Resolution Retinal Image Vessel Segmentation

Hasan Zengin[1], José Camara[2], Paulo Coelho[3,6(✉)], João M. F. Rodrigues[4], and António Cunha[5,6]

[1] Mehmet Akif Ersoy University, Burdur, Turkey
[2] Universidade Aberta, Porto, Portugal
[3] Polytechnic Institute of Leiria, Leiria, Portugal
paulo.coelho@ipleiria.pt
[4] LARSyS and ISE, Universidade do Algarve, Faro, Portugal
[5] University of Trás-os-Montes and Alto Douro, Vila Real, Portugal
acunha@utad.pt
[6] INESC TEC - Institute for Systems and Computer Engineering, Technology and Science, Porto, Portugal

Abstract. Segmentation process serves to aid the pathology diagnosing process since segmentation filters the interference from other anatomical structures and helps focus on the posterior segment structures of the eye, highlighting a set of signals that will serve for diagnosis of various retinal pathologies. Automatic retinal vessel segmentation can lead to a more accurate diagnosis. This paper presents a framework for automatic vessel segmentation of lower-resolution retinal images taken with a smartphone equipped with D-EYE lens. The framework is evaluated and the attained results were presented. A dataset was assembled and annotated of train models for automatic localisation retinal areas and for vessel segmentation. For the framework, two CNN based models were successfully trained, a Faster R-CNN that achieved a 96% correct detected of all regions with an MAE of 39 pixels, and a U-Net that achieved a DICE of 0.7547.

Keywords: Faster R-CNN · U-Net · Low-resolution retinal images · Segmentation · Screening

1 Introduction

Advances in science, especially in technological field, have improved the computing power of devices, and have enabled the development of information in medical imaging and medical diagnostics, the called Computer-Aided Diagnosis (CAD) systems, that can assist physicians in various tasks such as measuring anatomical structures, monitoring changes by comparing sequential images, diagnosing and planning treatment. They also prevent fatigue errors and increase work efficiency. In the ophthalmological field, such advances have enabled the primary

M. Antona and C. Stephanidis (Eds.): HCII 2020, LNCS 12189, pp. 611–627, 2020.
https://doi.org/10.1007/978-3-030-49108-6_44

prevention and early detection of pathologies that evolve asymptomatically and whose treatment may delay the deleterious effects of visual function. Many CAD systems are not yet used in clinical practice for several reasons. Claro et al. [5] discuss that retinal images that may have very different qualities due to various types of lesions and artefacts that make it difficult to design an image processing algorithm that is capable of handling a large number of retinal images. There are several algorithms for retinal image processing in the literature and different groups of researchers use different image bank metrics to track the performance of these algorithms, making it difficult to compare methods.

Retinal image became an important topic for the diagnosis serving as a diagnostic parameter for early and late retinal diseases as well as follow the evolution of numerous diseases such as diabetic retinopathy, hypertension, vascular diseases (arterial and venous occlusions), autoimmune diseases, glaucoma, senile macular degeneration, tumours, retinal detachment, among others.

In clinical practice, retinal structures may be visualized under myosis (undilated pupil) or mydriasis (artificially dilated pupil using anticholinergic and adrenergic drugs). The pupil represents a natural diaphragm of the eye that regulates the amount of external light and its diameter may vary from one individual to another. Viewing the retina under myosis allows for greater patient comfort but viewing a smaller fundus field. Visualization under mydriasis allows for a larger field of retinal visualization but may result in greater patient discomfort due to photophobia (increased sensitivity to external light) until the effect of instilled mydriatic drug decreases. To minimize and prevent the effects and pathology progression, laser therapy in the earliest stages of diabetic retinopathy is often recommended, although the success of such intervention depends on precocious detection and regular checkup/follow up by an ophthalmologist. Several methods have been proposed for early diagnosis of this disease [14] such as scanning laser ophthalmoscope, angiography, optical coherence tomography and fundus camera [13,15], which has been known as one of the primary methods for retinopathy screening [26]. Also, recent advances in image processing have promoted the diffusion of their application to several fields, including the areas of medical sciences, in particular, ophthalmology. A reliable procedure to evaluate retinopathies early is the structural analysis of retinal vessel network - the only blood vessel network of the body that is visible in a non-invasive imaging method [6]. Retinal images are taken with fundus cameras that produce high-quality and high-resolution retinal images for this analysis. Then, with vessel segmentation, interference from other anatomical structures are filtered, helping to obtain the focus of interest on posterior segment structures of the eye. This highlights a set of signals that will serve for diagnosis of various pathologies, such as, early changes in diabetic retinopathy (microaneurysms, microhemorrhages, cotton wool exudates), glaucoma (optic disc haemorrhages, delineation of the excavation and the outer limit of the optic papilla), and senile macular degeneration (coalescent druses, vascularization in the macular region). Manually segment retinal veins is a burdening task, highly time- and cost-consuming, therefore, investigations of automatic or semi-automatic methods for vessel segmentation have been evolving to assist specialists [2,20].

For treatment, early diagnosis has high-importance value. Detection needs regular retinal imaging, and this is a sort of process which is followed by taking high-resolution photos taken by expensive machines like fundus cameras, Optos UWF and Centervue's Eidon. However, the use of low-cost lenses using non-mydriatic pupils can bring several advantages besides economy, greater portability and ease of use and greater patient comfort, on the other hand, decreasing the quality of the photos obtained.

The latest trends in research show the extensive use of convolution neural networks (CNN) for the segmentation of retinal vessels and detection of the disease [7], beyond many other methods [20]. Nevertheless, a mutual aspect of the methods is that all focused on segmenting vessels with high-resolution retina images. The appearance of low-resolution retinal images obtained with low-cost devices suitable for the observation of retinal lesions is an opportunity to promote the dissemination of eye disease screening tests. The produced images have a small aperture and low quality. Although studies have already been published to prove the usefulness of these images, there is still a lack of studies to evaluate the effectiveness of automatic methods to segment retinal vessels in this type of image. These low-resolution and low-quality retinal images create extra difficulties in the use of traditional vessel segmentation methods [28].

This paper presents a framework focused on the vessels segmenting on lower-resolution retinal images taken with a smartphone equipped with D-EYE lens. The D-EYE [1] is a low-cost lens that can be attached to the lens of a smartphone to get undisturbed pupil background photos and videos with the added advantage of bringing more comfort to the patient with the disadvantage of not having the necessary sharpness when used in eyes with small pupils, in eyes with opacity of media (keratitis, cataract), in very bright environments, with the patient not collaborating. It is able to capture up to 20° under miosis at the posterior pole of the eye depending on individual pupil size.

A dataset was created with 26 retina videos around the optic disc, with lower-resolution images, and annotated two subsets, one with the localization of the retinal visible area and other with vessel segmentation. Here, a framework is proposed to provide the first step for a mobile solution to segment retinal vessels around the optic disc. The framework has two main steps: (a) The detection of the optic disc region using a Faster R-CNN and (b) visible vessel segmentation made by U-Net, trained with the mentioned dataset.

The main contributions of the paper are: (i) a low-resolution dataset created using D-EYE vessel annotation, (ii) a low-cost retinal vessel segmentation framework.

Section 2 presents and discusses the related work; Sect. 3 describes and illustrated the created dataset. Section 4 describes in detail the framework for low-resolution vessel segmentation, Sect. 5 presents the tests and attained results, and Sect. 6 finalizes the paper with discussion and conclusions.

2 Related Works

Image segmentation is the process of partitioning a digital image into multiple sets of pixels, in order to change its representation into something more meaningful and easier to analyze. Due to its wide range of applications, this process has become an attractive process in the image processing research area and, thus, a high number of algorithms have been developed over the years, including for the retinal vessel segmentation purpose.

Images used in published retinal vessel segmentation studies are taken with fundus cameras, that are expensive equipment that produces high-quality and high-resolution retinal images. The emergence of low-cost solutions, such as the taken from smartphones equipped with D-EYE [1], has given rise to evaluation and publications of their clinical employment. For example, in [28], a preference study was made between the use of a smartphone equipped with D-EYE lens and the use of the direct ophthalmoscope. 92% of the medical students that participated claimed their preference for use D-EYE. In [16], ophthalmologists deduced that smartphone captured fundus images are readable by experts, with an average between 86% and 100%, and they have an acceptable quality in 93%–100% for cataract patients. Vilela et al. [25] presented a meta-analysis study to check the agreement between retinal images obtained via smartphones and images obtained with retinal cameras or fundoscopic exams, claiming a very strong agreement between smartphone-based fundoscopic images and clinical examinations gold standards, so this resource can facilitate medical student learning and can also be an assessment for unprivileged or remote populations.

To the best of our knowledge, no studies have been published to evaluate vessel segmentation methods in low-resolution fundus images such as the taken from smartphones equipped with D-EYE.

The published methods for vessel segmentation of retinal images with high-quality and high-resolution retinal images use both supervised and unsupervised methods [2,10]. Supervised methods, such as support vector machine (SVM) and artificial neural network (ANN), have been used with a great impact on medical imaging segmentation and classification due to their increased performance. The unsupervised methods are used to discover hidden patterns from blood vessel from the retinal images [2]; they are out of the scope of this work.

Tuba et al. [23] proposed an overlapping block-based method characterised by SVM classification, whose features were obtained from discrete cosine transform (DCT) coefficients and chromaticity. Although this algorithm presents the advantage to classify large retinal vessels accurately, it is limited to classify thinner vessels. Wang et al. [27] proposed an algorithm where a vector containing 30 features of every pixel of the retinal image was formed containing features in Gaussian scale space, multiscale Gabor filter, and the vector field divergence. These feature vectors were then used as input to an SVM classifier. The authors claimed an improved segmentation performance and a reduced running time.

Jiang et al. [11] proposed a method that applies a deep fully convolutional neural networks (FCN), which integrate novel methods of data preprocessing, data augmentation, and full convolutional neural networks. The authors claim

that the proposed framework achieves state-of-the-art vessel segmentation performance in all three public benchmark tests, the datasets DRIVE [21], STARE [9] and CHASE_DB1 [17].

Some works are presented by applying the well-known U-Net [19] network and its modifications. Jin et al. [12] proposed deformable U-Net (DUNet) using U-shape structures and local features to perform retinal vessel segmentation in an end-to-end method. The up-sampling operators used in DUNet improve the output resolution, capture the contextual information, and to facilitate specific localization by combining both high- and low-level features. Another approach is LadderNet [29], which can be considered as a chain of multiple U-Nets and benefits from multiple paths of information flow, which provides the potential to capture more complicated features and produce a higher accuracy. Other authors proposed methods based on U-Net, both a Recurrent Convolutional Neural Network (RCNN) – RU-Net [3], where recurrent convolutions are applied before down-sampling, before up-sampling and before outputting the segmentation map, and also a Recurrent Residual Convolutional Neural Network (RRCNN) – R2U-Net [3], where residual learning is added to the convolutional unit.

3 Dataset

To train and evaluate the proposed platform, three datasets were used: dataset 1 (DS1), dataset 2 (DS2) and dataset 3 (DS3) - see Table 1.

Table 1. Image datasets used to train and evaluate the framework.

	DS1	DS2	DS3
Resolution (pixels)	1920×1080	320×320	80×80
Train	18 videos; 3,881 images (64%)	2 videos; 252 images (73%)	14 images; 1,967 patches (70%)
Validation	3 videos; 776 (13%)	1 video; 40 images (11%)	3 images; 421 patches (15%)
Test	5 videos; 1,375 images (23%)	1 video; 55 images (16%)	3 images; 422 patches (15%)
Total	26 videos; 6,060 images	4 videos; 347 images	20 images; 2,810 patches

A dataset of 26 low-resolution videos of the optic papilla under myosis (undilated pupil) was captured from the left and right eyes of 19 volunteers to train and evaluate this framework. The videos have an average of 15–20 s, were captured with an iPhone S6 with a D-EYE lens attached to the camera, present 1920×1080 pixels resolution at 15 frames per second. The videos obtained have

low quality due to factors such as light diffraction according to pupil size, media opacity, optical axis alignment, physiological eye intrinsic movements, and eyelid ptosis.

The videos were split into single images and organized in two different datasets, dataset1 (DS1) to be used in the detection of the retinal visible area, and the dataset2 (DS2) to be used in the segmentation of the retinal veins.

For the dataset1, the video-images were manually separated into two folders: "good images" when the retinal area and their veins are visible; and "bad images" for the remain. 4,657 images were selected and their retinal region labelled with the LabelImg software [24]. For the dataset2, 347 images were selected and manually segmented their veins with the labelling software Sensarea [4]. A square patched image was created based on the predicted outbox centre with 320×320 pixels and zeroing the out pixels of the image, as can be seen in Fig. 1.

Fig. 1. At left, a high-resolution retina image with the zoomed optic-disk; At right, a low-resolution retina image with a zoomed area of the retina, both from the same eye.

Additionally, as dataset3 (DS3), a training set of retina public dataset DRIVE: Digital Retinal Images for Vessel [21] was used for pre-training a segmentation CNN. It is composed of 20 colour images with 565×584 pixels acquired using a Canon CR5 non-mydriatic 3CCD camera with a 45-degree field of view (FOV) and their manual segmentation of the vasculature mask. Dataset2 images have larger dimensions than those in the DRIVE dataset. To adjust veins dimensions between both datasets, it was decided to obtain dataset2 patches subsample images with 80×80 pixels, as shown in Fig. 2.

Fourteen images were used for the train set (producing 1,967 patches), 3 for the validation (producing 421 patches), and 3 for the test set (producing 422 patches).

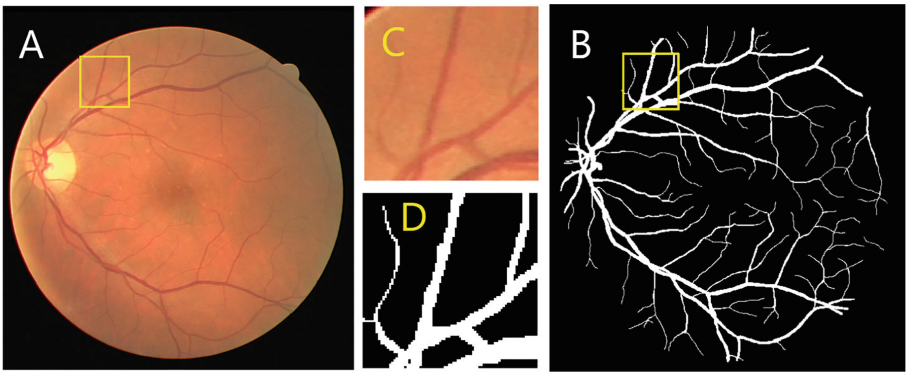

Fig. 2. Example of DRIVE dataset and patches created for dataset3: (A) retina image; (B) veins mask; (C) image patch; and (D) veins patch mask.

4 Framework for Low-Resolution Vessel Segmentation

The proposed framework for low-resolution vessel segmentation has two main steps (see Fig. 3): the (A) detection of the retinal visible area and the (B) vessel segmentation.

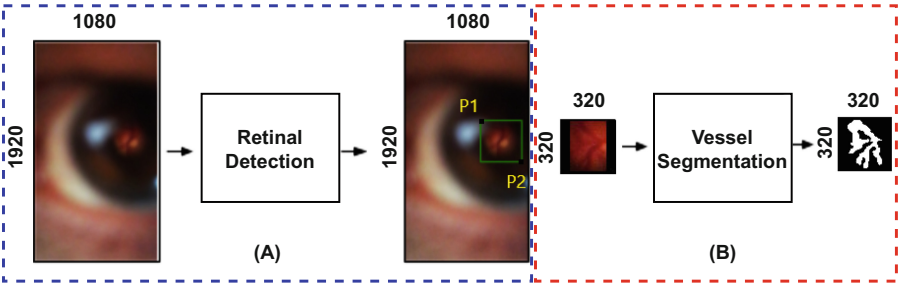

Fig. 3. Pipeline diagram for the proposed low-resolution vessel segmentation framework.

The detection of the retinal visible area (A) consists in to compute the location of a rectangle defined by P1 and P2, that encloses the visible area in the image (the area of interest). In this case, input images have 1920×1080 pixels, due to the D-EYE low lens aperture the area of interest has up to 320×320 pixels.

In this work, it was used a Faster R-CNN model although there is an enormous amount of object/region detection methods applied to computer science. Specifically, the Fast R-CNN [8] and the Faster R-CNN [18] were considered due to its low system requirements and fast computation for classifying object characteristics. Both models extract feature maps from the input image using CNN.

After this operation instead of selective search like in Fast R-CNN [8], in Faster R-CNN it takes region proposal network (RPN), that making this approach more advanced to feature extraction. Conceptually, Faster R-CNN is composed of 3 independent neural networks: the feature network (FN), the region proposal network (RPN) and the detection network (DN). The FN is applied to extract and produce relevant features from the images, so its output maintains the structure and shape of the original image. The RPN is usually constituted by a 3 convolutional layer network, where there is a common layer that feeds the following ones. One is used for classification purposes and the other for bounding box regression. The RPN main purpose is to generate a certain number of bounding boxes, with a high probability of containing an object. The DN takes input from both FN and RPN, and produces the final class and bounding box, being usually composed of 4 Fully Connected layers.

To evaluate the model, the Mean Absolute Error (MAE) defined in the Eq. 1 is a commonly used metric since it permits to measure the accuracy for continuous variables.

$$MAE = \frac{1}{N}\sum_{i=1}^{N} |y_i - \widehat{y}_i|\,, \tag{1}$$

where N is the number of variables, y_i is the ground truth value and $\widehat{y}_i$ is the predicted variable. In this case, it was used four variables, two for the coordinates of the upper left corner and the other two for the lower right corner.

The vessels segmentation (B) was done within the detected retinal areas, with a U-Net [19] model pre-trained with the dataset3 and tuned and evaluated with dataset2.

The U-Net [19] model was chosen due to its proven success for segmentation in the biomedical area. U-Net takes its name from the architecture shaped as 'U' letter. It is common in segmentation operations because of matching pooling and up-scaling layers. A given image will be applied to down-scaling for few-layer and up-scaling again for the same amount of layers which is used for down-scaling. Matching the output of 2 layers that are size partners of up-scale and down-scale layers makes the segmentation more successful.

To measure the success of the model, it was used the Dice Coefficient (DICE). The DICE is a relative metric that provides a similarity measure between predicted and ground truth segmentations, as defined in Eq. 2:

$$DICE = \frac{2 \cdot tp}{2 \cdot tp + fp + fn}, \tag{2}$$

where the *tp* are the total number of pixels belonging to the veins in both masks: predicted and ground truth, the *tn* are the total number of pixels that mutually don't belong to predicted and ground truth masks. The *fp* are the total number of pixels predicted as veins but are not present in the ground truth mask. The *tn* are the total number of pixels predicted as not belonging to veins but are present in the ground truth mask.

5 Tests and Results

The framework was evaluated for the retinal visible area detection and for vessels segmentation test sets described in Sect. 3.

Retinal Visible Area Detection
Faster R-CNN model was used to detect retinal visible area detection. It was implemented in TensorFlow, with features pre-trained with Inception Resnet V2 and fine-tuned with the private dataset1. For augmenting dataset1 were applied rotations with 90-degree steps. The model was trained with default parametrization: l2_regularizer of 0.01, truncated_normal_initilalizer of 0.01, maxpool_kernel_size of 2, maxpool_stride of 2, localization_loss_weight of 2, objectness_loss_weigh of 1, score_converter Softmax, momentum optimizer with learning rate 0.0002, momentum_optimizer_value of 0.9.

The Faster R-CNN obtained results for retinal visible area detection can be seen in Table 2.

Table 2. Testset evaluation of the Faster R-CNN model for retinal visible area detection.

Classification score	Frequency	P1 MAE (pixels)*	P2 MAE (pixels)*	P1 and P2 MAE (pixels)*
0.0	30 (2%)	311 (414)	252 (321)	281 (371)
0.1	4 (0%)	46 (28)	41 (20)	43 (25)
0.2	12 (1%)	63 (41)	40 (31)	51 (38)
0.3	6 (0%)	47 (27)	30 (8)	38 (22)
0.4	7 (1%)	37 (23)	41 (26)	39 (24)
0.5	11 (1%)	76 (69)	50 (37)	63 (57)
0.6	11 (1%)	91 (60)	37 (20)	64 (52)
0.7	14 (1%)	61 (62)	35 (26)	48 (49)
0.8	29 (2%)	67 (50)	36 (20)	52 (41)
0.9	1,251 (91%)	47 (49)	28 (13)	37 (37)
Total images	1,375			

* MAE: mean (standard deviation)

The results are organized in 10 classification scores with intervals of 0.1. The detection was very successful as 91% of the test images were detected with the classification score equal to or greater than 0.9. As the confidence score decrease, the MAE errors keep approximately constant until it reaches the score interval 0.0, where it increases for the mean of 281 and a standard deviation of 371. A closer look at the data (not in Table 2) showed that interval 0.8 has 29 images all with a score greater than 0.85.

In Figs. 4 and 5, it can be seen examples of the predicted areas (green boxes) and the ground truth areas (yellow boxes) in the best and the worst sum of error P1 and P2 in each interval.

In all the intervals the predicted area include the visible retinal area, with the exception of confidence interval 0.0 for the worst sum of error P1 and P2 (Fig. 4, last row), where the prediction selection is in the upper left corner of the image. However, even the best error P1 and P2 in interval 0.0 include the retinal area. All the best error prediction are very accurate when compared with ground truth. The worst cases include the retinal and some other retinal areas (that is, a retinal area not selected in the ground truth probably due to the variability of the observer who annotated the images). So on the one hand, it can be concluded that the detection area was very accurate. On the other hand, the confidence score seems to be related to the quality of the retinal area, and in the lower interval, the areas appear less good particularly in interval 0.0.

We considered reasonable to use a threshold above 0.5 to accept the areas as valid-regions, that in this case achieved 96% of correct detected for all regions, with MAE of 39 pixels.

Retinal Vessel Segmentation

The U-Net model was implemented using Keras, with a TensorFlow backend. For training the U-Net model, it was used the binary cross-entropy as loss function and Adam's optimiser with 10^{-3} learning rate based on Ange Tato and Roger Nkambou's work [22] used to achieve faster a stable convergence. ReLU function was used for the nine layers and in the output layer, the sigmoid activation function has applied.

The model was trained first with DS3 (Model 1), then trained on the join of DS2 and DS3 testsets (Model 2) and later retrained Model 1 with DS2 (Model 3) to tune the network with D-EYE retinal data. The attained results are summarized in Table 3.

Table 3. Results of the Model 1, Model 2 and Model 3.

	Model 1	Model 2	Model 3
(DS3) testset	0.7824	–	0.5784
(DS2 & DS3) testset	0.7474	0.7312	–
(DS2) testset	0.4797	0.7547	0.5580

Model 1 is has a reasonable Dice coefficient that seems adequate for the task (0.7824). Observing Fig. 6, it can be seen that the best result (first column) was achieved a DICE of 0.935 in a patch where vessels are wide and well visible. The model predictions (row 3) have the same structure but seems wider than the ground truth (row 2).

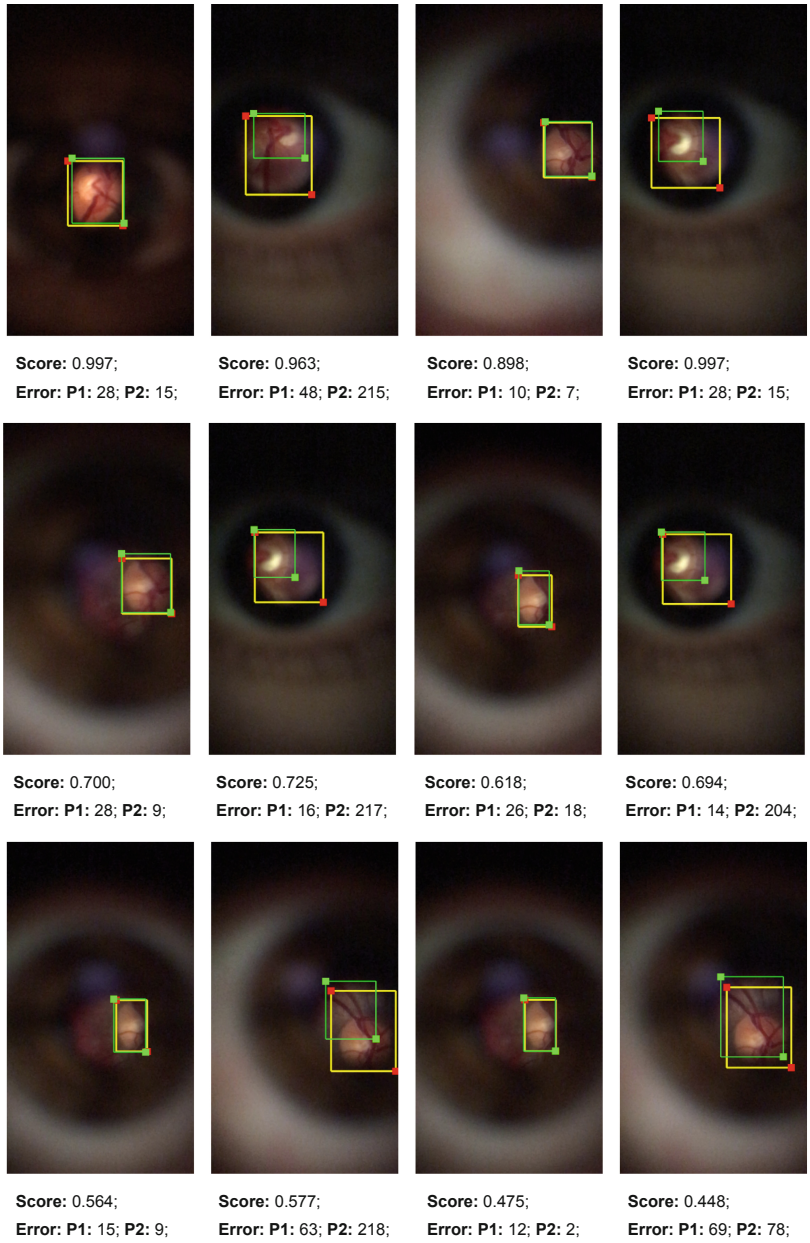

Fig. 4. Example of the best and the worst sum of errors P1 and P2 in intervals 0.9 and 0.8 (first row), 0.7 and 0.6 (second row) and 0.5 and 0.4 (third row). (Color figure online)

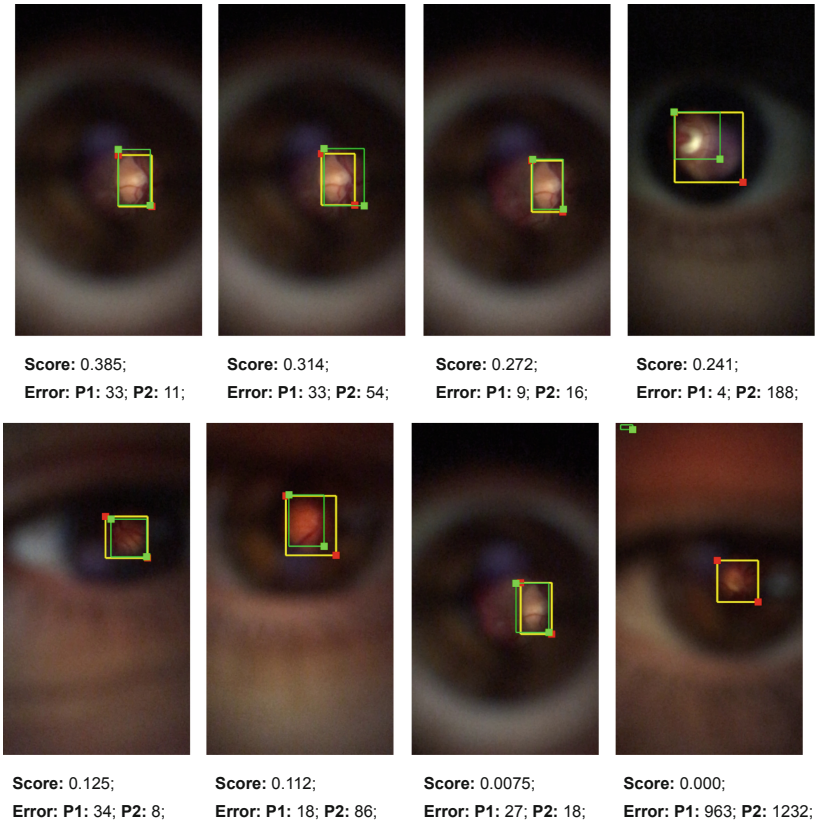

Fig. 5. Example of the best and the worst sum of errors P1 and P2 in intervals 0.3 and 0.2 (first row), 0.1 and 0.0 (second row). (Color figure online)

At the second column, it can be seen the worst prediction (DICE of 0.0512). At the original image, vessels are thin, almost imperceptible and quite different from the vessels expected to find in low-resolution images. It was selected another image patch with thin veins that seems to us more similar to the ones expected (third column). In this case, the predicted image preserves the structure, it also seems wider than the ground-truth and achieved a DICE of 0.8571.

To observe how the model Model 1 performs with the low-resolution images, it was evaluated in the DS2 testset, obtaining a low DICE value (0.4797). In the fourth and fifth columns of Fig. 6, it can be seen the best and worst predictions. Both patch images are very dark and veins are poorly visible - the image-patch of fifth is the poorest. The best-predicted segmentation (DICE of 0.8009) is actually very good, considering the visibility of the veins and though the difficulty of manually creating the ground-truth.

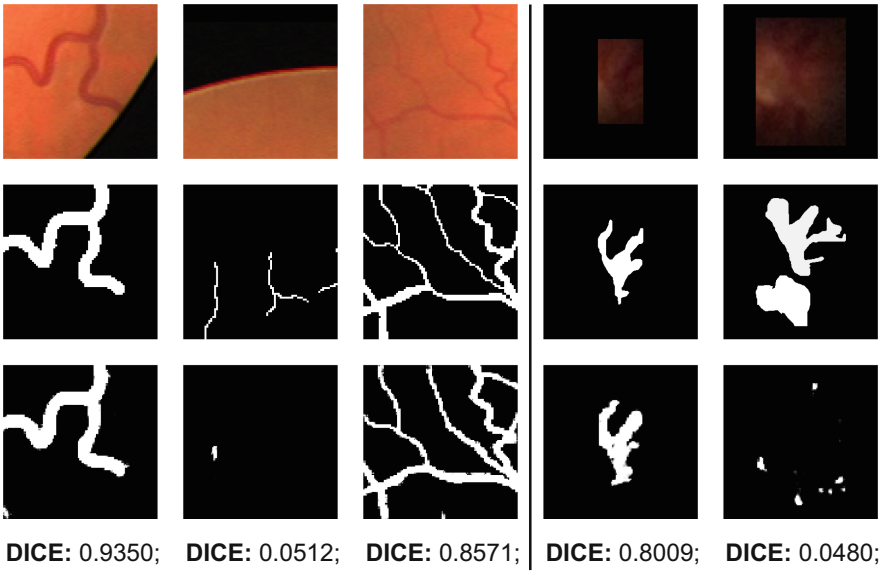

Fig. 6. Example of image patches predicted with U-Net Model 1. The first row, original patches: the first three are from DS3 testset, respectively best, worst and reasonable predictions; and the last two from DS2 testset, respectively best and worst predictions. The second row, ground truth patches, and the third row, Model 1 predictions. (Color figure online)

The Model 2 achieved a DICE of 0.7312 on the join of DS2 and DS3 testsets that is lower than the obtained for Model 1 (DICE of 0.7474), but it achieved better on the DS2 testset (DICE of 0.7547). Examples of predicted images of Model 2 can be seen in Fig. 7.

To illustrate the Model 2 predictions of dataset DS2 testset, were chosen four images: the best prediction (DICE: 0.7510), two in-between predictions (DICE: 0.6054, DICE: 0.5100) and the worst prediction (DICE: 0.4304). For comparison with Model 1, column 5 has the predict results of the worst-patch image predicted by Model 1 (see Fig. 6, column 5). It can be seen that segmentations are much better: in the first two cases, the structure is all connected as in ground-truth, the other two (where veins are less visible in patch images) have several discontinuities in the structure. In column 5, ones can see that the Model 2 produces a much better segmentation (DICE: 0.4304) than the produced by Model 1 (see Fig. 6, lower right image).

The last tests made were for Model 3, by doing a posterior train of Model 1 with DS2, but the results were worse than with Model 1.

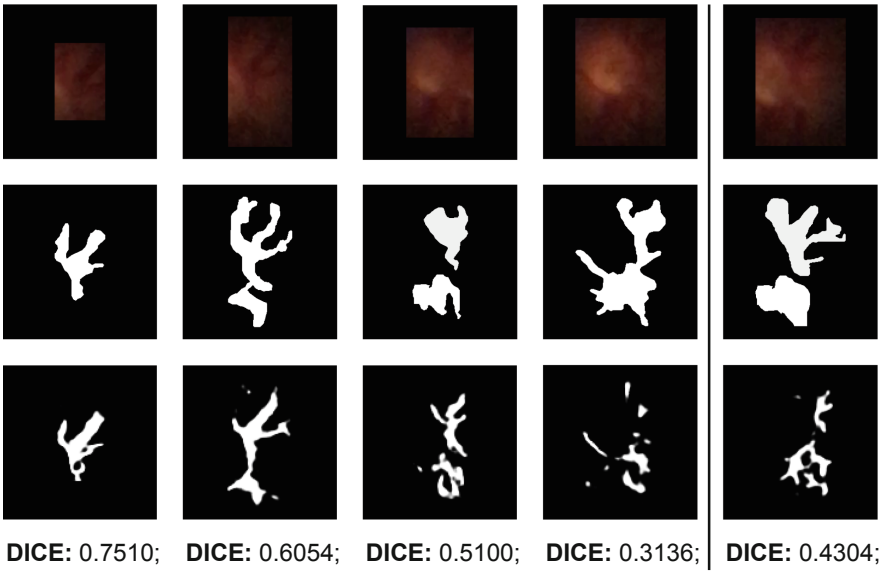

Fig. 7. Example of image patches predicted with U-Net Model 2. The first row, original patches: the first four are from DS2 testset, respectively best, two in-between, and worst predictions; and for comparison, the worst case of Model 1 low-resolution prediction, is presented in the last column. The second row, ground truth patches, and the third row, Model 2 predictions.

6 Discussion and Conclusions

In this paper, a framework for vessels segmenting on lower-resolution retinal images was proposed, evaluated and the attained results were presented. A dataset of train models was assembled and annotated for automatic localization of retinal areas and for vessel segmentation. For the framework, two CNN-based models were successfully trained, a Faster R-CNN that achieved a 96% correct detection of all regions with an MAE of 39 pixels, and a U-Net that achieved a DICE of 0.7547. This study is precursor to future works to the determination of eye diseases, such as glaucoma and diabetes, applied to low-resolution images.

Acknowledgments. This project was financed by the Portuguese funding agency, FCT - Fundação para a Ciência e a Tecnologia, through national funds, and co-funded by the FEDER, where applicable.

This paper is financed by LARSyS - FCT Plurianual funding 2020–2023.

References

1. D-Eye Web Site. https://www.d-eyecare.com/en_PT/product
2. Almotiri, J., Elleithy, K., Elleithy, A.: Retinal vessels segmentation techniques and algorithms: a survey. Appl. Sci. **8**(2), 155 (2018). https://doi.org/10.3390/app8020155. http://www.mdpi.com/2076-3417/8/2/155
3. Alom, M.Z., Hasan, M., Yakopcic, C., Taha, T.M., Asari, V.K.: Recurrent residual convolutional neural network based on U-Net (R2U-Net) for medical image segmentation (February 2018). http://arxiv.org/abs/1802.06955
4. Bertolino, P.: SENSAREA, a general public video editing application. In: 21st IEEE International Conference on Image Processing (ICIP 2014). IEEE, Paris (October 2014). https://hal.archives-ouvertes.fr/hal-01080565
5. Claro, M., Veras, R., Santos, L., Frazão, M., Carvalho Filho, A., Leite, D.: Métodos computacionais para segmentação do disco óptico em imagens de retina: uma revisão. Revista Brasileira de Computação Aplicada **10**(2), 29–43 (2018). https://doi.org/10.5335/rbca.v10i2.7661. http://seer.upf.br/index.php/rbca/article/view/7661
6. Fraz, M.M., Rudnicka, A.R., Owen, C.G., Strachan, D.P., Barman, S.A.: Automated arteriole and venule recognition in retinal images using ensemble classification. In: Proceedings of the 9th International Conference on Computer Vision Theory and Applications, vol. 3, pp. 194–202. SCITEPRESS - Science and and Technology Publications (2014). https://doi.org/10.5220/0004733701940202
7. Gargeya, R., Leng, T.: Automated identification of diabetic retinopathy using deep learning. Ophthalmology **124**(7), 962–969 (2017). https://doi.org/10.1016/j.ophtha.2017.02.008. https://linkinghub.elsevier.com/retrieve/pii/S0161642016317742
8. Girshick, R.: Fast R-CNN. In: 2015 IEEE International Conference on Computer Vision (ICCV), vol. 2015 Inter, pp. 1440–1448. IEEE (December 2015). https://doi.org/10.1109/ICCV.2015.169. http://ieeexplore.ieee.org/document/7410526/
9. Hoover, A., Kouznetsova, V., Goldbaum, M.: Locating blood vessels in retinal images by piecewise threshold probing of a matched filter response. IEEE Trans. Med. Imaging **19**(3), 203–210 (2000). https://doi.org/10.1109/42.845178. http://ieeexplore.ieee.org/document/845178/
10. Imran, A., Li, J., Pei, Y., Yang, J.J., Wang, Q.: Comparative analysis of vessel segmentation techniques in retinal images. IEEE Access **7**, 114862–114887 (2019). https://doi.org/10.1109/ACCESS.2019.2935912. https://ieeexplore.ieee.org/document/8804190/
11. Jiang, Y., Zhang, H., Tan, N., Chen, L.: Automatic retinal blood vessel segmentation based on fully convolutional neural networks. Symmetry **11**(9), 1112 (2019). https://doi.org/10.3390/sym11091112. https://www.mdpi.com/2073-8994/11/9/1112
12. Jin, Q., Meng, Z., Pham, T.D., Chen, Q., Wei, L., Su, R.: DUNet: a deformable network for retinal vessel segmentation. Knowl.-Based Syst. **178**(8), 149–162 (2019). https://doi.org/10.1016/j.knosys.2019.04.025. https://linkinghub.elsevier.com/retrieve/pii/S0950705119301984
13. Jones, N.P., Sala-Puigdollers, A., Stanga, P.E.: Ultra-widefield fundus fluorescein angiography in the diagnosis and management of retinal vasculitis. Eye **31**(11), 1546–1549 (2017). https://doi.org/10.1038/eye.2017.93. http://www.nature.com/articles/eye201793

14. MacGillivray, T.J., Trucco, E., Cameron, J.R., Dhillon, B., Houston, J.G., van Beek, E.J.R.: Retinal imaging as a source of biomarkers for diagnosis, characterization and prognosis of chronic illness or long-term conditions. Br. J. Radiol. **87**(1040), 20130832 (2014). https://doi.org/10.1259/bjr.20130832. http://www.birpublications.org/doi/10.1259/bjr.20130832
15. McGrory, S., et al.: The application of retinal fundus camera imaging in dementia: a systematic review. Alzheimer's Dement.: Diagn. Assess. Dis. Monit. **6**, 91–107 (2017). https://doi.org/10.1016/j.dadm.2016.11.001
16. Mohammadpour, M., Heidari, Z., Mirghorbani, M., Hashemi, H.: Smartphones, tele-ophthalmology, and VISION 2020. Int. J. Ophthalmol. **10**(12), 1909–1918 (2017). https://doi.org/10.18240/ijo.2017.12.19. http://www.ijo.cn/gjyken/ch/reader/viewabstract.aspx?fileno=20171219&flag=1
17. Owen, C.G., et al.: Measuring retinal vessel tortuosity in 10-year-old children: validation of the computer-assisted image analysis of the retina (CAIAR) program. Investig. Opthalmol. Vis. Sci. **50**(5), 2004 (2009). https://doi.org/10.1167/iovs.08-3018. http://iovs.arvojournals.org/article.aspx?doi=10.1167/iovs.08-3018
18. Ren, S., He, K., Girshick, R., Sun, J.: Faster R-CNN: towards real-time object detection with region proposal networks. IEEE Trans. Pattern Anal. Mach. Intell. **39**(6), 1137–1149 (2017). https://doi.org/10.1109/TPAMI.2016.2577031. http://ieeexplore.ieee.org/document/7485869/
19. Ronneberger, O., Fischer, P., Brox, T.: U-Net: Convolutional networks for biomedical image segmentation. In: Navab, N., Hornegger, J., Wells, W.M., Frangi, A.F. (eds.) MICCAI 2015. LNCS, vol. 9351, pp. 234–241. Springer, Cham (2015). https://doi.org/10.1007/978-3-319-24574-4_28
20. Singh, N., Kaur, L.: A survey on blood vessel segmentation methods in retinal images. In: 2015 International Conference on Electronic Design, Computer Networks & Automated Verification (EDCAV), pp. 23–28. IEEE (January 2015). https://doi.org/10.1109/EDCAV.2015.7060532. http://ieeexplore.ieee.org/document/7060532/
21. Staal, J., Abramoff, M., Niemeijer, M., Viergever, M., van Ginneken, B.: Ridge-based vessel segmentation in color images of the retina. IEEE Trans. Med. Imaging **23**(4), 501–509 (2004). https://doi.org/10.1109/TMI.2004.825627. http://ieeexplore.ieee.org/document/1282003/
22. Tato, A., Nkambou, R.: Workshop track -ICLR 2018 Improving Adam Optimizer, pp. 1–4 (2018)
23. Tuba, E., Mrkela, L., Tuba, M.: Retinal blood vessel segmentation by support vector machine classification. In: 2017 27th International Conference Radioelektronika (RADIOELEKTRONIKA), pp. 1–6. IEEE (April2017). https://doi.org/10.1109/RADIOELEK.2017.7936649. http://ieeexplore.ieee.org/document/7936649/
24. Tzutalin, D.: LabelImg (2015). https://github.com/tzutalin/labelImg
25. Vilela, M.A.P., Valença, F.M., Barreto, P.K.M., Amaral, C.E.V., Pellanda, L.C.: Agreement between retinal images obtained via smartphones and images obtained with retinal cameras or fundoscopic exams – systematic review and meta-analysis. Clin. Ophthalmol. **12**, 2581–2589 (2018). https://doi.org/10.2147/OPTH.S182022. https://www.dovepress.com/agreement-between-retinal-images-obtained-via-smartphones-and-images-o-peer-reviewed-article-OPTH
26. Viswanath, K., McGavin, D.D.M.: Diabetic retinopathy: clinical findings and management. Community Eye Health **16**(46), 21–4 (2003). http://www.ncbi.nlm.nih.gov/pubmed/17491851

27. Wang, Y.B., Zhu, C.Z., Yan, Q.F., Liu, L.Q.: A novel vessel segmentation in fundus images based on SVM. In: 2016 International Conference on Information System and Artificial Intelligence (ISAI), pp. 390–394. IEEE (June 2016). https://doi.org/10.1109/ISAI.2016.0089. http://ieeexplore.ieee.org/document/7816742/
28. Wu, A.R., Fouzdar-Jain, S., Suh, D.W.: Comparison study of funduscopic examination using a smartphone-based digital ophthalmoscope and the direct ophthalmoscope. J. Pediatr. Ophthalmol. Strabismus **55**(3), 201–206 (2018). https://doi.org/10.3928/01913913-20180220-01
29. Zhuang, J.: LadderNet: multi-path networks based on U-Net for medical image segmentation, pp. 2–5 (October 2018). http://arxiv.org/abs/1810.07810